GA–A22636

RECENT H–MODE DENSITY LIMIT EXPERIMENTS ON DIII–D

by
M.A. MAHDAVI, R. MAINGI, R.J. LA HAYE, T.C. JERNIGAN,
T.W. PETRIE, L.R. BAYLOR, A.W. HYATT, A.W. LEONARD,
M. MURAKAMI, L.W. OWENS, R.T. SNIDER, R.D. STAMBAUGH,
M.R. WADE, J.G. WATKINS, W.P. WEST, D.G. WHYTE, R.D. WOOD
and the DIII–D TEAM

JUNE 1997

DISCLAIMER

GA–A22636

RECENT H–MODE DENSITY LIMIT EXPERIMENTS ON DIII–D

by
M.A. MAHDAVI, R. MAINGI,[†] R.J. LA HAYE, T.C. JERNIGAN,[†]
T.W. PETRIE, L.R. BAYLOR,[†] A.W. HYATT, A.W. LEONARD,
M. MURAKAMI, L.W. OWENS,[†] R.T. SNIDER, R.D. STAMBAUGH,
M.R. WADE,[†] J.G. WATKINS,[#] W.P. WEST, D.G. WHYTE,[Δ] R.D. WOOD[◊]
and the DIII–D TEAM

This is a preprint of a paper to be presented at the Twenty-Fourth European Conference on Controlled Fusion and Plasma Physics, June 9–14, 1996, Berchtesgaden, Germany, and to be published in the *Proceedings*.

[†]Oak Ridge National Laboratory
[#]Sandia National Laboratories
[Δ]University of California, San Diego
[◊]Lawrence Livermore National Laboratory

Work supported by
the U.S. Department of Energy
under Contract Nos. DE-AC03-89ER51114,
DE-AC05-96OR22464, DE-AC04-AL85000, W-7405-ENG-48,
and Grant No. DE-FG03-95ER54294

GA PROJECT 3466
JUNE 1997

RECENT H–MODE DENSITY LIMIT EXPERIMENTS ON DIII–D*

M.A. Mahdavi, R. Maingi,† R.J. La Haye, T.C. Jernigan,† T.W. Petrie, L.R. Baylor,† A.W. Hyatt, A.W. Leonard, M. Murakami,† L.W. Owens,† R.T. Snider, R.D. Stambaugh, M.R. Wade,† J.G. Watkins,# W.P. West, D.G. Whyte,Δ R.D. Wood,◊ and The DIII–D Team
General Atomics, P.O. Box 85608, San Diego, California 92186-5608 USA

A vast body of tokamak data [1–4] is in good agreement with the empirical density limit scalings proposed by Hugill and Greenwald. These are of the form $n_{Hugill} \sim B/Rq$ and $n_{GW} \sim I_p/\pi a^2$, respectively, which differ only in the elongation dependence, roughly $(1 + \kappa^2)/2$, implicit in the definition of the safety factor q. These scalings have common puzzling features of showing no dependence on either impurity concentration or heating power, since the density limit is frequently correlated with a rapid rise of the edge radiation. Despite the resiliency of these scalings, several machines under restrictive conditions have operated at densities well above the predictions of these scalings, albeit with pellet injection and at varying degrees of confinement degradation. Furthermore, data from several machines display a weak dependence on heating power. These results cast doubt on the universal validity of both of these scalings. Nevertheless the fact remains that access to densities above Hugill-Greenwald scaling is very difficult. A number of theories [5–8] based on radiative power balance in the plasma boundary have explained some but not all features of tokamak density limit behavior, and as ITER design studies recently brought to focus, a satisfactory understanding of this phenomenon is lacking. Motivated by a need for better understanding of effects of density and fueling on tokamak plasmas in general, we have conducted a series of experiments designed to identify and isolate physical effects suspected to be directly or indirectly responsible for the density limit. The physical effects being considered include: divertor power balance, MARFE [9,10], poloidally symmetric radiative instabilities, MHD instabilities, and transport. In this paper we will first present a brief summary of the experimental results up to the writing of this paper. The remainder of the paper is devoted to a comparison of our data at the onset of the MARFE instability with predictions of theory and the implication of the results on access to densities beyond the Hugill-Greenwald limit.

Normally, in DIII–D, with either gas or pellet fueling, a density limit in the range 0.7–1.1 Greenwald limit is observed. This limit is seen following divertor detachment when the most prominent radiation zone reaches the X-point, and is attributed to the divertor power balance limit. We were able to bypass this limit [3] by lowering the SOL density relative to the line average density. This was achieved by simultaneous divertor pumping and pellet injection. The main difficulties encountered in increasing the density beyond this point were associated with deleterious effects of injection of large pellets (D = 2.7 mm, $\delta N/N \approx 30\%$), as described in the following paragraph. Once these problems were resolved, densities well above n_{GW} were accessed. As shown in Fig. 1, in H–mode plasmas densities = $1.5 \times n_{GW}$ were

*Work supported by the U.S. Department of Energy under Contract Nos. DE-AC03-89ER51114, DE-AC05-96OR22464, DE-AC04-94AL850000, W-7405-ENG-48, and Grant No. DE-FG03-95ER54294.
†Oak Ridge National Laboratory, Oak Ridge, Tennessee.
#Sandia National Laboratories, Livermore, California.
ΔUniversity of California, San Diego, California.
◊Lawrence Livermore National Laboratory, Livermore, California.

maintained for several hundred milliseconds. In the discharge shown in Fig. 1, global energy confinement time peaked at the ITER93-H–mode scaling level before decaying due to high radiation from the plasma core. Strong attenuation of the neutral heating beam was a main contributor to the ultimate central radiation collapse. It is important to note that the density profiles in these plasmas were only moderately peaked, as the line average density was only 50% above the H–mode pedestal value a few centimeters inside the separatrix.

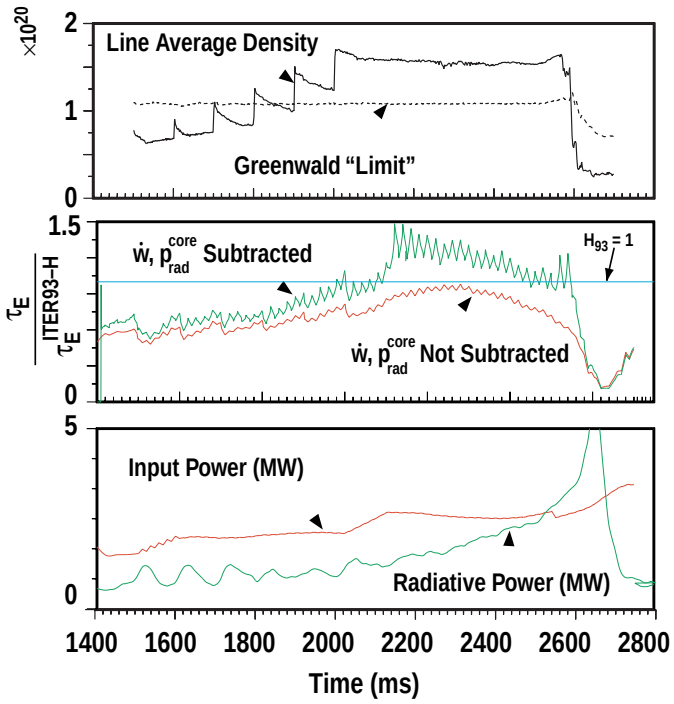

Fig. 1. H–mode confinement, $\gtrsim \tau_E^{ITER-93H}$, at $\bar{n}_e = 1.5\, n_{GW}$ is attained. Excessive radiation from plasma center degrades confinement, and ultimately leads to radiative collapse.

Pellets invariably triggered low mode number rotating MHD modes which greatly complicated access to high densities. These modes often reduced energy and particle confinement back to L–mode levels and occasionally locked and caused disruptions. Occasionally the modes continued to grow long after the pellet density perturbation had decayed away and when the current profile appeared to be stable to classical and neoclassical tearing modes. Furthermore, at times, the modes stabilized after further density increase. The initial excitation of these modes might be explained by the large adiabatic temperature perturbation at low rational surfaces; however additional physics is needed to explain their continued growth when the current profile seems to be stable. A phenomenon similar to the m=1, n=1, "snake" mode [11] is suspected, and is the subject of continuing investigation.

Several other deleterious effects of pellet fueling were observed which reduced the attainable parameter window for high density plasmas. First, spontaneous or pellet triggered ELMs expelled a large fraction of the plasma density which frequently increased the fueling demand beyond the available injection rate. This problem was mitigated only by lowering the ELM frequency through lowering the heating power relative to the plasma current, since the ELM frequency scales with P_{INJ}/I_p^2. Second, near the H–mode power threshold, pellets caused transient H-L transitions, which also caused unacceptable particle loss. This problem was avoided by lowering B_T since the power threshold scales linearly with B_T.

The MARFE condensation instability is a density dependent phenomenon which has been suspected to be the cause of the density limit in tokamaks. Figure 2 shows data from two discharges, one with q_{95} = 9, in which a MARFE occurred at a line density of 5×10^{19} corresponding to ~0.8 n_{GW}. The second discharge with q_{95} = 3.2 reached a line density of 1.8×10^{20}, corresponding to $2 \times n_{GW}$ up to the symmetric radiation limit without MARFE formation. This comparison suggests that the normally observed tokamak density limit is not due to MARFE instability. However, a closer examination shows that the same procedures

used to access high densities may have stabilized the MARFE in the high density discharge. The MARFE marginal stability condition is given by [6]:

$$\kappa_{\perp}\left(\frac{\partial^2 \tilde{T}}{\partial r^2}\right) - \kappa_{||}\left[\frac{\tilde{T}}{(qR)^2}\right] \cong n_e^2\, T^2 \sum_I \frac{n_I}{n_e}\frac{d}{dT}\left[\frac{1}{T^2} L_I\left(T, \frac{n_0}{n_e}\right)\right]\tilde{T} \quad , \qquad (1)$$

where $\tilde{T}$ is the temperature perturbation, $L(T, n_o/n_e)$ is the radiation rate, and $\kappa_{||} = (\kappa_0/Z_{eff})\, T^{5/2}$ is the Spitzer parallel conductivity. The right hand side of the equation represents the radiation destabilizing term. The left hand side terms are owing to perpendicular and parallel conduction, respectively, and are both stabilizing. We have tested the plasma parameters of the discharges of Fig. 2 against this criterion, using coronal equilibrium radiation rates from ADPAK [12]. The first term on the left was ignored, since for radial scale lengths >1 cm and $\kappa_{\perp} \cong 7 \times 10^{16}$ erg cm^{-1} eV^{-1} [13], the second term dominates. Then Eq. (1) reduces to

$$\left\{\sum_I \frac{n_e}{n_I}\left(\frac{1}{\sqrt{T}}\right)\frac{d}{dT}\left[L_I\left(T, \frac{n_o}{n_e}\right)\right]\right\}^{-1/2} \geq \left(qR\sqrt{\frac{Z_{eff}}{\kappa_o}}\right) n_e \quad \text{(for stability)} \qquad (2)$$

In Fig. 3 we have plotted the left hand side of Eq. (2) for measured impurity concentrations of 1% carbon and 0.06% oxygen. The solid curve corresponds to the coronal equilibrium [$(n_o/n_e) = 10^{-7}$]. The dashed curve incorporates the nonequilibrium effect of a uniform neutral distribution of $n_o/ne = 10^{-3}$. Modeling [14] by B2.5 and DEGAS codes show that a neutral concentration of this magnitude exists between $\rho = 0.99$ and $\rho = 1$ radii. Open circles in the figure represent the RHS of Eq. (2) using data for the discharge with MARFE before the MARFE formation. For this discharge, three points, $\rho = 0.96$–0.99, are near or inside the unstable zone. In contrast for the discharge with no MARFE formation (solid diamonds), all experimental points are well within the stable zone. Although in this analysis, the oxygen concentration is more than a factor of ten lower than that of carbon, since the oxygen radiation peak occurs at a higher temperature than carbon, oxygen is a significant contributor to instability. The stability diagram of Fig. 3 demonstrates the critical importance of boundary plasma temperature. In the temperature range of 10 to 100 eV the stability threshold increases rapidly with T_e. Above 100 eV, the temperature dependence is weak but the density ceiling in this region is high compared to normal tokamak operating densities. Thus in the divertor configuration an effective way of increasing the MARFE threshold is by increasing the separatrix temperature through SOL density control, as was done in present experiments.

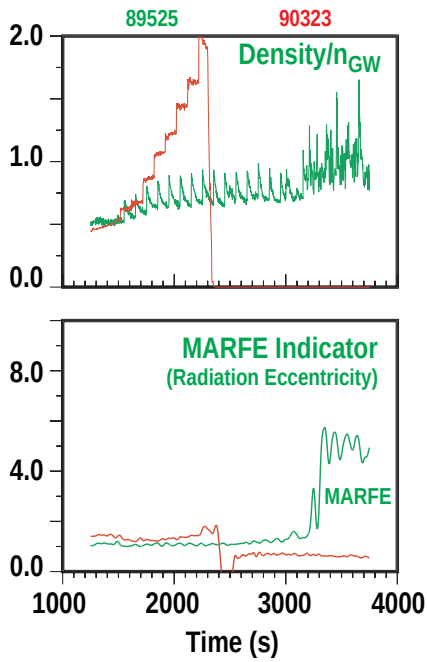

Fig. 2. Solid curve: example of high density H–mode shots with no MARFE formation [$\bar{n}_e(\max) = 1.8 \times 10^{20}$ m$^{-3} \cong 2$ n_{GW}, I_p = 1.3 MA]. The dashed curve shows a high q L–mode edge plasma with MARFE formation at low density [$\bar{n}_e(\max) = 0.6 \times 10^{20}$ m$^{-3} \cong$ 0.8 n_{GW}, I_p = 0.7 MA].

A power law fit to the LHS of Eq. (2) shows that the local MARFE stability limit for oxygen impurity in coronal equilibrium in the 30–100 eV range scales as $n_{crit} \sim T_e^4/qR[(n_I/n_e)Z_{eff}]^{0.5}$. Now we wish to eliminate T_e in favor of n_e. We define the pressure profile factor $g(\rho)$ by $n(\rho)T(\rho) \equiv g(\rho)\langle p\rangle$. By substituting for $\langle p\rangle$ from the definition $\tau_E \equiv 1.5\langle p\rangle V/P$, where V is the plasma volume, we obtain $T(\rho) \sim g(\rho)\tau_E/Vn(\rho)$. Now using the $\tau_E = \tau_E^{ITER\text{-}89P}$ confinement scaling, we obtain a local MARFE threshold scaling of the form:

$$n_{crit}(\rho) \sim g(\rho)^{0.8}\, I_p^{0.96}\, a^{-1.9}\, \xi^{-0.11}\, P^{0.17}\, R^{0.17}\, B^{0.04}\left[\kappa^2\left(1+\kappa^2\right)\right]^{-0.22} \quad .$$

This result with an approximate I/a^2 scaling, is remarkably insensitive to oxygen concentration and B_T, and has weak dependencies on heating power, elongation, and major radius, and might explain the origin of the Hugill-Greenwald scalings. The scaling shows that since the inner plasma has a much higher MARFE limit, the global MARFE limit can be increased by density peaking. In the divertor configuration, however, as discussed above, it is possible to maintain the separatrix temperature high and thus achieve high line average densities without density peaking.

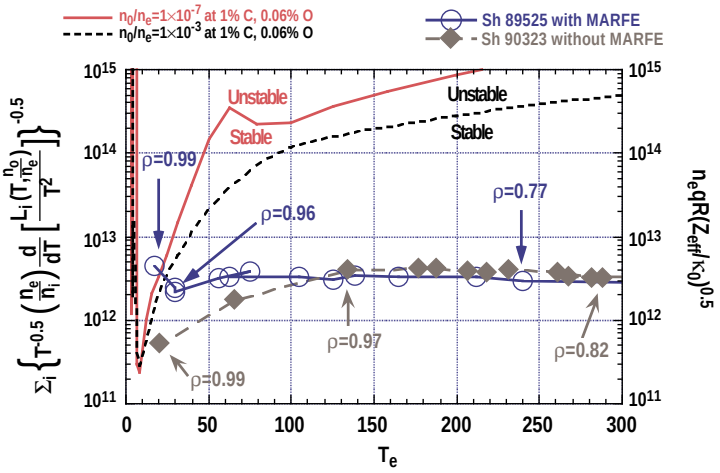

Fig. 3. Comparison of edge plasma parameters measured just inside the separatrix with the MARFE threshold criteria. The solid curve represents calculated value of LHS of Eq. (2) for coronal equilibrium. The dashed curve incorporates radiation enhancement due to a neutral concentration of $n_o/n_e = 10^{-3}$. The open circles represent the experimental values for the RHS of Eq. (2) for the discharge with MARFE formatrion, the solid diamonds correspond to the discharge that reached $n_e = 2 \times n_{GW}$ without MARFE formation.

In summary, we have demonstrated compatibility of high confinement at densities above the Hugill-Greenwald limit without strong density peaking. An explanation for the origin of Hugill and Greenwald scalings is offered which is based on the MARFE instability. We conclude that ITER, with a separatrix temperature of $\gtrsim$ 150 eV, can safely access densities well above the Greenwald limit without MARFE instability.

[1] Hugill, S., Proc. 2nd Joint Varenna-Grenoble Symp., Brussels, 775 (1980).
[2] Greenwald, M., et al., Nucl. Fusion **28**, 2199 (1988).
[3] Maingi, R., et al., Phys. Plasmas **4**, 1752 (1997), and references thereof.
[4] Petrie, T.W., et al., Nucl. Fusion **33**, 929 (1993).
[5] Drake, J., Phys. Fluids **30**, 8 (1987).
[6] Wesson, J.A., and Hender, T.C., Nucl. Fusion **33**, 1019 (1993).
[7] Ohyabu, N., Nucl. Fusion **19**, 1491 (1979).
[8] Borras, K., Nucl. Fusion **31**, 1035 (1991).
[9] Baker, D.R. , et al., Nucl. Fusion **22**, 807 (1982).
[10] Lipschultz, B., et al., Nucl. Fusion **22**, 977 (1984).
[11] Wesson, J.A., Plasma Physics and Controlled Fusion **37**, 337 (1995).
[12] Hulse, R., et al., Nucl. Techn./Fusion **3**, 259 (1983).
[13] Porter, G.D., et al., Phys. Plasmas **3**, 1967 (1996).